Thermal Fly-height Control Slider Instability and Dynamics at Touchdown: Explanations using Nonlinear Systems Theory

Sripathi V Canchi* and David B Bogy

Computer Mechanics Laboratory

Mechanical Engineering

University of California, Berkeley, CA, USA

Abstract

Thermal Fly-height Control sliders are widely used in current hard disc drives to control and maintain sub-nanometer level clearance between the read-write head and the disc. The peculiar dynamics observed during touchdown/contact tests for certain slider designs is investigated through experiments and analytical modeling. Nonlinear systems theory is used to highlight slider instabilities arising from an unfavorable coupling of system vibration modes through an internal resonance condition, as well as the favorable suppression of instabilities through a jump condition. Excitation frequencies that may lead to large amplitude slider vibrations, and the dominant frequencies at which slider response occurs are also predicted from theory. Using parameters representative of the slider used in experiments, the theoretically predicted frequencies are shown to be in excellent agreement with experimental results. This analytical study highlights some important air bearing surface design considerations that can help in the prevention of slider instability as well as help in the mitigation of unwanted slider vibrations thereby ensuring the reliability of the head disc interface at extremely low head-disc clearances.

* E-mail: vcsripathi@berkeley.edu; 5146 Etcheverry Hall, Berkeley CA 94720

I. INTRODUCTION

In order to achieve the target storage density of $10Tb/in^2$ in hard disc drives a physical clearance of $0.25nm$ between the head and the disc media is required. Currently, Thermal Fly-height Control (TFC) architecture is used to achieve sub-nanometer clearance between the read-write head and the disc. Power supplied to the TFC heater deforms the slider body locally near the read-write head through resistive heating thereby providing the actuation necessary for spacing control. In practice, the read-write head to disc clearance is calibrated against the heater power by determining the touch-down power (TDP), i.e. the power to achieve zero-clearance or slider contact with the lubricant on the disc. The TDP together with the knowledge of the slider's thermal actuation efficiency (fly-height loss per milliwatt, known from slider and heater design) is used to calculate and supply the appropriate heater power to achieve a desired head-disc clearance during operation.

Slider dynamics at touchdown/contact and proximity (near contact conditions) have been studied in the past and are ongoing topics of investigation. The motivation arises from the need to understand the effect of intermittent as well as continuous contact on slider dynamics in three dimensions (vertical, down-track and off-track), as well as to develop advanced techniques to accurately detect touchdown/contact in experiments and in a working hard disc drive. Experiments have focused on studying the slider's flying characteristics and contact induced dynamics using disc RPM spin-down tests for traditional sliders and thermal protrusion controlled touchdown tests for TFC sliders [1–5]. Extensive literature on experimental as well as computational work quantifying the effects of various nonlinear forces at the HDI (intermolecular, electrostatic, lubricant adhesion, and contact forces) on the slider dynamics for low-flying and partial contact sliders is available [6–12]. Enhanced slider-lubricant interactions at low spacing and contact is known to cause lubricant rippling, lubricant pick-up from the disc to the slider and subsequent lubricant drop-off from the slider onto the disc proving detrimental to the slider dynamics as well as overall head-disk interface (HDI) reliability [13–18].

Recently, the possibility of having a slider in continuous contact with the lubricant has received considerable attention. Experimental investigations previously reported by the authors [19] show peculiar results for slider dynamics in TFC actuated contact with the disc lubricant. Slider-lubricant contact at TDP causes significant vibrations (instability)

in the vertical, down-track and off-track directions. For particular slider designs, however, this vibration suddenly gets suppressed (stability) above a critical heater power beyond the TDP. While this stable condition is attributed to a lube-surfing regime [20], the physics behind this phenomena is not fully understood. Modeling efforts considering the static case show that stable flying-heights are possible under lubricant contact due to the nonlinearity of the external forces (the net effect of air bearing pressure, adhesion, contact, etc.) [21, 22] but these results do not readily extend to the dynamic case where the external forces also vary with time. Numerical simulations for the dynamic case can predict the slider motions for particular sets of HDI parameters and initial conditions for a chosen nonlinear model [23, 24], but they are inadequate for explaining the origin and physics of the problem.

This paper reports continued investigations on the topic of slider instability and dynamics at touchdown/contact through experiments and analytical modeling. Experiments reveal that the frequency spectrum of slider vibrations at touchdown consists of peaks at the first pitch mode, its harmonics, and additionally, several peaks at frequencies lower and higher than the first pitch mode. A simple analytical model which accounts for thermal protrusion and the special dynamic case of periodic external forcing is used to predict and offer explanations for slider instability and response observed in the experiments. The slider is represented by a two-degree of freedom model (accounting for the vertical and pitch motions), and the load carrying air-bearing surface (ABS) is represented by two springs, one each for the leading and trailing ends. The thermal protrusion is modeled as a relative change in the nonlinear stiffness of the trailing end spring, compared to the linear stiffness of the leading end spring. The coupled nonlinear equations for slider motion are derived and studied analytically using nonlinear systems theory.

Thermal protrusion continuously changes the system natural frequencies through the change in the trailing end stiffness, and interesting slider dynamics occur for particular protrusion ranges. Large amplitude vibrations (instability) as well as their suppression (stability) observed in experiments may be explained by phenomena characteristic to nonlinear systems. In particular, the coupling of vibration modes through an *internal resonance* condition is discussed as a cause for slider instability. Nonlinear systems theory also offers a prediction of excitation frequencies that lead to large amplitude response and a prediction of frequencies in the ensuing response. The frequency peaks in slider response obtained from experiments are well accounted for by theory, and they correspond to the primary and

combination resonance conditions resulting in *subharmonics*, *superharmonics* and *fractional harmonics* of the nonlinear system.

II. EXPERIMENTS

Experiments are performed with 'pemto' TFC sliders ($1.25mm \times 0.84mm$) on a $95mm$ media coated with PFPE lubricant. The spin stand is instrumented with a laser doppler vibrometer (LDV) to measure slider's vertical vibration, an acoustic emission (AE) sensor to monitor contact at the HDI and an *in-situ* optical surface analyzer (OSA) to investigate changes to the lubricant surface (Fig 1). A custom built Labview code together with a data acquisition board and amplifier circuit is used to input pre-programmed power profiles to the TFC heater with submilliwatt resolution. The test procedure is as follows: The slider is loaded onto the rotating disc and moved to the desired track. The touchdown power (TDP) is measured using the automated Labview program which uses AE signal as feedback and records the power at which there is a sudden change in the AE signal as the TDP [19]. Once the TDP is determined, the transient slider dynamics under contact are investigated by supplying a power profile that consists of four sinusoidal waves having a $1s$ time period [19]. The peak power of this waveform is TDP+$20mW$ in these investigations. All tests are conducted at 0^o skew and at the slider's design linear velocity of $22m/s$.

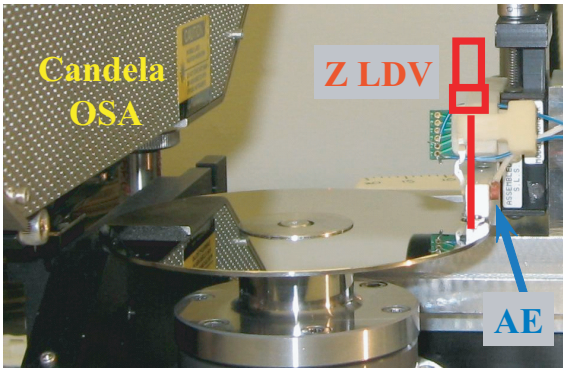

FIG. 1. Spin stand set-up with Candela OSA, AE sensor and LDV

The time history of the slider's vertical velocity, AE signal and supplied heater power are shown in Fig 2 for the first cycle of the sinusoidal power waveform. For this particular air bearing surface (ABS) design (shown in Fig 2), peculiar dynamics are observed during the transient test. The slider shows significant vibrations (denoted as the 'unstable' region)

when the heater power is increased slightly above the TDP. However, when the heater power is increased above a critical power beyond the TDP, the slider vibrations as well as AE signal are suddenly suppressed (denoted as the 'stable' region). Previous researchers have speculated that this condition of suppressed vibrations corresponds to a case of lube-surfing, where a small portion of the thermal protrusion is in continuous contact with the lubricant [20, 23]. However, the authors of this paper have shown that the evidence from *in-situ* lubricant scans support the distinct possibility of the slider flying at a secondary stable flying-height without lubricant-contact at higher heater powers [19]. Further investigations are ongoing to fully understand the physics of this phenomenon.

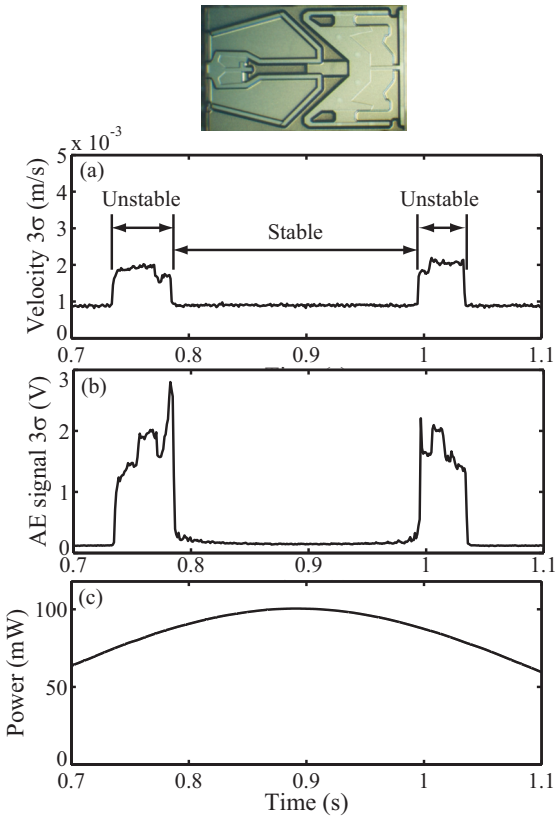

FIG. 2. Experimental result for the 'pemto' slider: Time history of (a) slider's vertical velocity 3σ (b) AE signal 3σ (c) power supplied to TFC heater

The current experiments also reveal that the frequency spectrum of slider vibrations at TDP (unstable region) consists of peaks at the first pitch mode ($128kHz$), its harmonics, and additionally, several peaks at frequencies lower and higher than the first pitch mode (Fig 3). The appearance of multiple peaks in the frequency spectrum highlight the effect

of nonlinearities, and similar results have been reported for traditional (non-TFC) sliders in proximity from experiments and simulation [6]. Motivated by this observation, the slider-ABS nonlinear system is analytically investigated with a focus on understanding whether it is possible for the slider to have 'unstable' dynamics for certain range(s) of heater power (i.e. thermal protrusion), whether slider dynamics could be rendered 'stable' because of interacting nonlinearities, and whether the experimentally observed peaks in the frequency spectrum of slider vibrations are explained by theory.

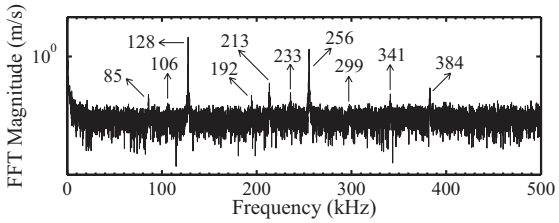

FIG. 3. Frequency spectrum of the slider's vertical velocity in the 'unstable' zone

III. ANALYTICAL MODEL

The slider is modeled as a rigid body with only two degrees of freedom, corresponding to the pitch and vertical motion. The air bearing is represented by springs and dampers, one each for the trailing and leading ends (Fig 4). The spring at the trailing end is assumed to be nonlinear (with quadratic and cubic terms) accounting for air bearing stiffness changes due to spacing changes from the slider vibrations as well as other nonlinearities at the HDI, such as those arising from electrostatic forces, intermolecular forces and slider contact with the lubricant or disc, to mention a few. Since the focus of this work remains on understanding the effect of nonlinearities on slider dynamics and stability, it is not of concern as to where these nonlinearities arise, but only that they are represented by quadratic and cubic terms as an approximation, thus keeping the math tractable. Thermal protrusion is modeled as an increase in the stiffness of the spring at the trailing end compared to the fixed stiffness of the spring at the leading end (through a multiplicative factor α) as explained in the subsequent section.

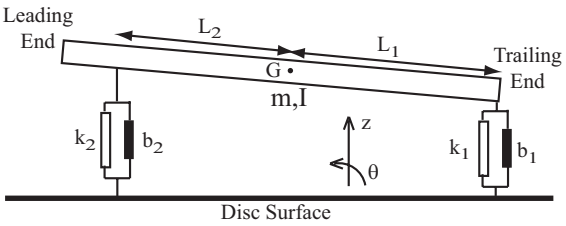

FIG. 4. Schematic of the two degree of freedom model for slider-ABS system

A. Equations of Motion

The equations of motion for the system (Fig 4) are easily derived using Lagrange's equations or other techniques. Assuming the leading and trailing end spring stiffnesses to have the form

$$\begin{aligned} k_1 &= k_{11} - k_{12}z + k_{13}z^2 \\ k_2 &= k_{21} \end{aligned} \tag{1}$$

the nondimensional equations of motion appear as

$$\begin{aligned} \ddot{\zeta} &= F_1 - \zeta - \Lambda_1 \sin\theta - \delta_1\dot{\zeta} - \delta_2\dot{\theta}\cos\theta \\ &\quad + \Lambda_4\zeta^2 - \Lambda_5\zeta^3 + \Lambda_6\zeta\sin\theta - \Lambda_7\zeta^2\sin\theta \end{aligned} \tag{2a}$$

$$\begin{aligned} \ddot{\theta} &= F_2 - \Lambda_1\zeta\cos\theta - \Lambda_2\sin\theta\cos\theta - \delta_2\dot{\zeta}\cos\theta - \delta_3\dot{\theta}\cos^2\theta \\ &\quad + \Lambda_6\zeta^2\cos\theta - \Lambda_7\zeta^3\cos\theta + \Lambda_8\zeta\sin\theta\cos\theta - \Lambda_9\zeta^2\sin\theta\cos\theta \end{aligned} \tag{2b}$$

where the dot implies derivatives with respect to the nondimensional time τ, ζ is the nondimensional displacement in the vertical direction, θ is the pitch angle, and the other quantities are related to the system parameters by

$$\begin{aligned} \tau &= \omega t & \zeta &= \frac{z}{L} & \omega^2 &= \frac{k_{11}+k_{21}}{m} \\ \Lambda_1 &= \frac{k_{11}l_1 - k_{21}l_2}{mL\omega^2} & \Lambda_2 &= \frac{k_{11}l_1^2 + k_{21}l_2^2}{mL^2\omega^2} & \Lambda_3 &= \frac{I}{mL^2} \\ \Lambda_4 &= \frac{k_{12}}{m\omega^2} & \Lambda_5 &= \frac{k_{13}L^2}{m\omega^2} & \Lambda_6 &= \frac{k_{12}l_1}{m\omega^2} \\ \Lambda_7 &= \frac{k_{13}l_1L}{m\omega^2} & \Lambda_8 &= \frac{k_{12}l_1^2}{m\omega^2} & \Lambda_9 &= \frac{k_{13}l_1^2}{m\omega^2} \\ \delta_1 &= \frac{b_1+b_2}{m\omega} & \delta_2 &= \frac{b_1l_1 - b_2l2}{mL\omega} & \delta_3 &= \frac{b_1l_1^2 + b_2l_2^2}{mL^2\omega} \\ F_1 &= \frac{F}{mL\omega^2} & F_2 &= \frac{M}{mL^2\omega^2} \end{aligned} \tag{3}$$

where m and I represent the slider's mass and moment of inertia, respectively, F and M represent the force and moment about the slider's center of mass G, respectively, and L is an arbitrary length scale (chosen to be $1nm$ unless mentioned otherwise). Note that the model is set-up such that $(\zeta, \theta) = (0, 0)$ is the equilibrium state. (In reality, the slider has a non-zero pitch at equilibrium, but can be neglected in this work for convenience and to keep the math tractable).

Since the range of pitch motion during slider vibration is very small (a few *microradians*), the approximations $\sin\theta \approx \theta$ and $\cos\theta \approx 1$ are valid, and the equations of motion (2) may be written in matrix form after making these approximations as

$$\mathbf{M}\ddot{\mathbf{x}} + \mathbf{C}\dot{\mathbf{x}} + \mathbf{K}\mathbf{x} + \mathbf{h}(\mathbf{x}) = \mathbf{F} \tag{4}$$

$$\mathbf{M} = \begin{pmatrix} 1 & 0 \\ 0 & \Lambda_3 \end{pmatrix} \qquad \mathbf{C} = \begin{pmatrix} \delta_1 & \delta_2 \\ \delta_2 & \delta_3 \end{pmatrix} \qquad \mathbf{K} = \begin{pmatrix} 1 & \Lambda_1 \\ \Lambda_1 & \Lambda_2 \end{pmatrix}$$

$$\mathbf{x} = \begin{pmatrix} \zeta \\ \theta \end{pmatrix} \qquad \mathbf{h}(\mathbf{x}) = \begin{pmatrix} h_1(\zeta, \theta) \\ h_2(\zeta, \theta) \end{pmatrix} \qquad \mathbf{F} = \begin{pmatrix} F_1 \\ F_2 \end{pmatrix}$$

$$h_1(\zeta, \theta) = \Lambda_4\zeta^2 + \Lambda_6\zeta\theta - \Lambda_5\zeta^3 - \Lambda_7\zeta^2\theta$$
$$h_2(\zeta, \theta) = \Lambda_6\zeta^2 + \Lambda_8\zeta\theta - \Lambda_7\zeta^3 - \Lambda_9\zeta^2\theta$$

The nonlinearities of the quadratic and cubic forms are evident and contained in $\mathbf{h}(\mathbf{x})$.

Considering only the linear part of (4), the natural frequencies ω_1 and ω_2 (also called the linear natural frequencies, where $\omega_1 < \omega_2$) and mode shapes are easily computed for a chosen set of system parameters through an eigenvalue analysis. The slider-ABS system has two modes: the ABS first pitch mode corresponding to ω_1 is the motion of the slider about a point close to the trailing end, while the ABS second pitch mode corresponding to ω_2 is the motion of the slider about a point closer to the leading end (Fig 5a).

In this work, the system parameters are chosen to match the slider used in the experiment. The slider's mass and moment of inertia are readily calculated from the slider's dimensions and material density (Table I) and the spring stiffness values are chosen so that the first pitch mode frequency matches the experimentally observed value of $128kHz$ for this slider. Accordingly, the stiffness value $k_{21} = 3.3 \times 10^5 N/m$ is used, while the stiffness value k_{11},

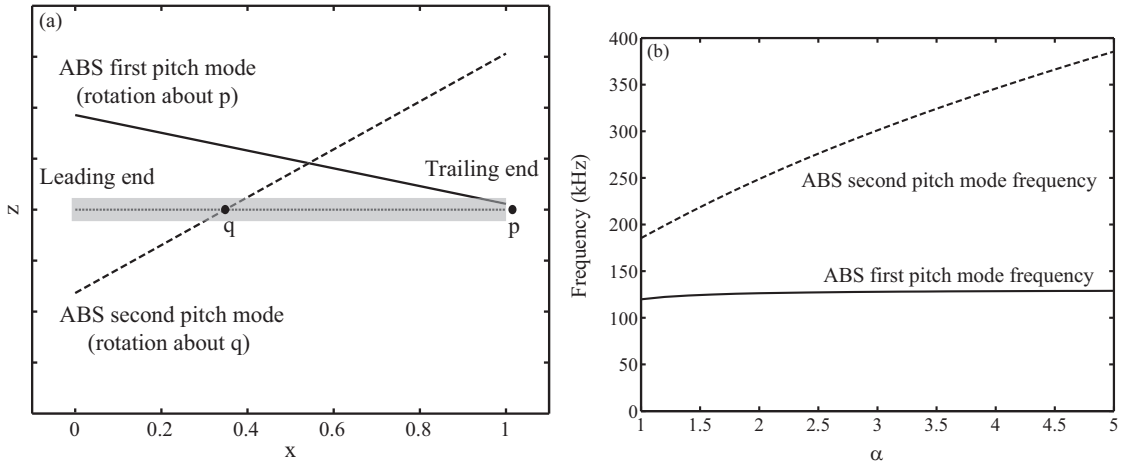

FIG. 5. Linear model analysis: (a) ABS first and second pitch mode shapes (b) first and second pitch mode frequencies as a function of thermal protrusion 'α'

which depends on the thermal protrusion is given by $k_{11} = \alpha k_{21}$ where $\alpha(> 1)$ increases with increasing protrusion.

The effect of thermal protrusion on the linear natural frequencies (ω_1, ω_2) is shown in Fig 5b. It is evident that increasing α (i.e. the thermal protrusion) does not change the first pitch mode frequency ω_1 significantly. However, the second pitch mode frequency ω_2 increases monotonically with α. It is verified that the mode shapes (Fig 5a) are not significantly altered by a change in α.

It is well known from nonlinear systems theory that when the linear natural frequencies of a two degree of freedom nonlinear system are commensurable or nearly commensurable, a strong coupling of the (otherwise decoupled) modes can occur, and this condition is called an internal resonance [25]. The occurrence of an internal resonance depends strongly on the system parameters, and the commensurability conditions for a two degree of freedom system are given by $\omega_2 \approx 2\omega_1$ when quadratic nonlinearities are present, and $\omega_2 \approx 3\omega_1$ when cubic nonlinearities are present.

Considering the slider-ABS system, based on the preceding calculations for ω_1 and ω_2 as a function of α, it is possible that for particular slider designs that have $\omega_1 < \omega_2 < 2\omega_1$ with no thermal protrusion (i.e. zero heater power), the thermal protrusion induced by increasing heater power can cause ω_2 to increase through an internal resonance condition ($\omega_2 \approx 2\omega_1$ or $\omega_2 \approx 3\omega_1$). For example, Fig 5b shows that $\omega_2 \approx 2\omega_1$ when $\alpha \approx 2.075$ and $\omega_2 \approx 3\omega_1$ when $\alpha \approx 5$ for the system parameters shown in Table I. An internal resonance could result

System Parameter	Value
Slider density (ρ)	$4425kg/m^3$
Slider length (L_s)	$1.33mm$
Slider width (w_s)	$0.83mm$
Slider height (h_s)	$0.23mm$
L_1	$L_s/2$
L_2	$0.75\ L_s/2$
k_{21}	$3.3 \times 10^5 N/m$
k_{11}	$\alpha k_{21}\ N/m$
k_{12}	$5 \times 10^7 k_{11}\ N/m^2$
k_{13}	$10^{15} k_{11}\ N/m^3$
$\hat{\mu}_1$	$0.01\omega_1$ (1%)
$\hat{\mu}_2$	$2\mu_1$
F	$2.3\ mN$
M	FL_1

TABLE I. System parameters

in large amplitude response depending on the system parameters. Therefore, for particular ranges of heater power, when an internal resonance condition occurs, large amplitude slider vibrations are possible, and they can lead to slider-lubricant/disc contact, or enhance the degree of existing slider-lubricant/disc contact.

The nonlinear equations (4) for the slider-ABS system are investigated for internal resonance and large amplitude response. This paper presents results only for the internal resonance condition $\omega_2 \approx 2\omega_1$ arising from quadratic nonlinearities. The analysis when $\omega_2 \approx 3\omega_1$ may be treated in a similar fashion [25].

B. Analysis of the Nonlinear Equations

The equations of motion are transformed and written in terms of the modal coordinates η and ϕ as

$$\ddot{\eta} + \omega_1^2 \eta = -2\hat{\mu}_1 \dot{\eta} + A_1\eta^2 + A_2\eta\phi + A_3\phi^2 + B_1\eta^3 + B_2\eta^2\phi + B_3\eta\phi^2 + B_4\phi^3 + \hat{F}_1 \tag{5a}$$

$$\ddot{\phi} + \omega_2^2 \phi = -2\hat{\mu}_2 \dot{\phi} + A_4\eta^2 + A_5\eta\phi + A_6\phi^2 + B_5\eta^3 + B_6\eta^2\phi + B_7\eta\phi^2 + B_8\phi^3 + \hat{F}_2 \tag{5b}$$

$$\begin{aligned}
A_1 &= \gamma_1(\Lambda_4\gamma_1^2 + \Lambda_6\gamma_1\gamma_3) + \gamma_3(\Lambda_6\gamma_1^2 + \Lambda_8\gamma_1\gamma_3) \\
A_2 &= \gamma_1(\Lambda_4 2\gamma_1\gamma_2 + \Lambda_6(\gamma_1\gamma_4 + \gamma_2\gamma_3)) + \gamma_3(\Lambda_6 2\gamma_1\gamma_2 + \Lambda_8(\gamma_1\gamma_4 + \gamma_2\gamma_3)) \\
A_3 &= \gamma_1(\Lambda_4\gamma_2^2 + \Lambda_6\gamma_2\gamma_4) + \gamma_3(\Lambda_6\gamma_2^2 + \Lambda_8\gamma_2\gamma_4) \\
A_4 &= \gamma_2(\Lambda_4\gamma_1^2 + \Lambda_6\gamma_1\gamma_3) + \gamma_4(\Lambda_6\gamma_1^2 + \Lambda_8\gamma_1\gamma_3) \\
A_5 &= \gamma_2(\Lambda_4 2\gamma_1\gamma_2 + \Lambda_6(\gamma_1\gamma_4 + \gamma_2\gamma_3)) + \gamma_4(\Lambda_6 2\gamma_1\gamma_2 + \Lambda_8(\gamma_1\gamma_4 + \gamma_2\gamma_3)) \\
A_6 &= \gamma_2(\Lambda_4\gamma_2^2 + \Lambda_6\gamma_2\gamma_4) + \gamma_4(\Lambda_6\gamma_2^2 + \Lambda_8\gamma_2\gamma_4)
\end{aligned} \tag{6}$$

$$\begin{aligned}
B_1 &= -\gamma_1(\Lambda_5\gamma_1^3 + \Lambda_7\gamma_1^2\gamma_3) - \gamma_3(\Lambda_7\gamma_1^3 + \Lambda_9\gamma_1^2\gamma_3) \\
B_2 &= -\gamma_1(\Lambda_5 3\gamma_1^2\gamma_2 + \Lambda_7(2\gamma_1\gamma_2\gamma_3 + \gamma_1^2\gamma_4)) - \gamma_3(\Lambda_7 3\gamma_1^2\gamma_2 + \Lambda_9(2\gamma_1\gamma_2\gamma_3 + \gamma_1^2\gamma_4)) \\
B_3 &= -\gamma_1(\Lambda_5 3\gamma_1\gamma_2^2 + \Lambda_7(2\gamma_1\gamma_2\gamma_4 + \gamma_2^2\gamma_3)) - \gamma_3(\Lambda_7 3\gamma_1\gamma_2^2 + \Lambda_9(2\gamma_1\gamma_2\gamma_4 + \gamma_2^2\gamma_3)) \\
B_4 &= -\gamma_1(\Lambda_5\gamma_2^3 + \Lambda_7\gamma_2^2\gamma_4) - \gamma_3(\Lambda_7\gamma_2^3 + \Lambda_9\gamma_2^2\gamma_4) \\
B_5 &= -\gamma_2(\Lambda_5\gamma_1^3 + \Lambda_7\gamma_1^2\gamma_3) - \gamma_4(\Lambda_7\gamma_1^3 + \Lambda_9\gamma_1^2\gamma_3) \\
B_6 &= -\gamma_2(\Lambda_5 3\gamma_1^2\gamma_2 + \Lambda_7(2\gamma_1\gamma_2\gamma_3 + \gamma_1^2\gamma_4)) - \gamma_4(\Lambda_7 3\gamma_1^2\gamma_2 + \Lambda_9(2\gamma_1\gamma_2\gamma_3 + \gamma_1^2\gamma_4)) \\
B_7 &= -\gamma_2(\Lambda_5 3\gamma_1\gamma_2^2 + \Lambda_7(2\gamma_1\gamma_2\gamma_4 + \gamma_2^2\gamma_3)) - \gamma_4(\Lambda_7 3\gamma_1\gamma_2^2 + \Lambda_9(2\gamma_1\gamma_2\gamma_4 + \gamma_2^2\gamma_3)) \\
B_8 &= -\gamma_2(\Lambda_5\gamma_2^3 + \Lambda_7\gamma_2^2\gamma_4) - \gamma_4(\Lambda_7\gamma_2^3 + \Lambda_9\gamma_2^2\gamma_4)
\end{aligned} \tag{7}$$

where ω_1 and ω_2 are the linear natural frequencies, $\hat{\mu}_1$ and $\hat{\mu}_2$ represent the modal damping values (the damping matrix $\mathbf{C}$ is diagonalized by the modal matrix $\mathbf{V}$ by an assumption of Raleigh damping), and $\mathbf{V}$ is given by

$$\mathbf{V} = \begin{pmatrix} \gamma_1 & \gamma_2 \\ \gamma_3 & \gamma_4 \end{pmatrix}; \qquad \begin{pmatrix} \zeta \\ \theta \end{pmatrix} = \mathbf{V} \begin{pmatrix} \eta \\ \phi \end{pmatrix}; \qquad \begin{pmatrix} \hat{F}_1 \\ \hat{F}_2 \end{pmatrix} = \mathbf{V}^T \begin{pmatrix} F_1 \\ F_2 \end{pmatrix} \tag{8}$$

The coupled equations (5) are in their simplest form accounting for the most general case of quadratic and cubic nonlinearities.

Considering the forcing term to be sinusoidal in nature, the nonlinear coupled equations (5) are analyzed using the method of multiple scales closely following the methods outlined

in [25]. The first order uniform solution of the form

$$\eta = \epsilon\eta_1 + \epsilon^3\eta_3 \tag{9a}$$

$$\phi = \epsilon\phi_1 + \epsilon^3\phi_3 \tag{9b}$$

is sought, where ϵ is a small parameter. Defining the different time scales $T_0 = t$, $T_2 = \epsilon^2 t$, and $D_k = \frac{d}{dT_k}$ for $k = 1, 3, \ldots$ the time derivative is represented by

$$\frac{d}{dt} = D = D_0 + \epsilon^2 D_2 + \ldots \tag{10a}$$

$$\frac{d^2}{dt^2} = D^2 = D_0^2 + \epsilon^2 2D_0 D_2 + \ldots \tag{10b}$$

In the following analysis, two cases require slightly different consideration: the primary resonance case, when the frequency of the forcing term (Ω) is close to one of the system linear natural frequencies ω_1 or ω_2, and the secondary resonance (or nonresonant) case, when Ω is far away from ω_1 or ω_2.

1. *Primary Resonance ($\Omega \approx \omega_1$)*

The primary resonance condition considered in this work corresponds to $\Omega \approx \omega_1$, such as that occurring when the lubricant is rippled at the first pitch mode and feeds into system excitation and resonance [14]. Strictly speaking, the forcing term is also dependent on the system state variables $(\zeta, \theta, \dot{\zeta}, \dot{\theta})$, however, the analysis is simplified by assuming that the forcing term is independent of state variables and dependent exclusively on time.

The scaling of quantities is to be chosen such that the forcing term, the nonlinearities and the damping interact at the same order. In the problem of slider vibration with small amplitudes (onset of instability), the damping and quadratic terms are of comparable order, while the cubic terms are of higher order. However, when the vibration amplitudes grow to become sufficiently large, the cubic terms can have the same order as the quadratic and damping terms. In order to simplify the analysis, it is assumed that quadratic as well as cubic nonlinearities are of the same order, corresponding to the case of large amplitude slider vibrations. The solution for the case where cubic terms are absent is easily found by setting the coefficients corresponding to the cubic terms to zero. Accordingly, the ordering

of quantities is given by

$$\hat{\mu}_i = \epsilon^2 \mu_i \qquad A_j = \epsilon \alpha_j \qquad B_k = \beta_k \qquad \hat{F}_i = \epsilon^3 f_i \cos(\Omega t + \tau_i)$$
$$i = 1, 2 \; ; \quad j = 1, 2 \ldots, 6 \; ; \quad k = 1, 2, \ldots, 8 \tag{11}$$

Substituting (9), (10), (11) into (5), and collecting terms of order ϵ and order ϵ^3 gives

$$D_0^2 \eta_1 + \omega_1^2 \eta_1 = 0 \tag{12a}$$

$$D_0^2 \phi_1 + \omega_2^2 \phi_1 = 0 \tag{12b}$$

$$\begin{aligned} D_0^2 \eta_3 + \omega_1^2 \eta_3 = & -2 D_0 D_2 \eta_1 - 2 \mu_1 D_0 \eta_1 + \alpha_1 \eta_1^2 + \alpha_2 \eta_1 \phi_1 + \alpha_3 \phi_1^2 \\ & + \beta_1 \eta_1^3 + \beta_2 \eta_1^2 \phi_1 + \beta_3 \eta_1 \phi_1^2 + \beta_4 \phi_1^3 + f_1 cos(\Omega T_0 + \tau_1) \end{aligned} \tag{13a}$$

$$\begin{aligned} D_0^2 \phi_3 + \omega_2^2 \phi_3 = & -2 D_0 D_2 \phi_1 - 2 \mu_2 D_0 \phi_1 + \alpha_4 \eta_1^2 + \alpha_5 \eta_1 \phi_1 + \alpha_6 \phi_1^2 \\ & + \beta_5 \eta_1^3 + \beta_6 \eta_1^2 \phi_1 + \beta_7 \eta_1 \phi_1^2 + \beta_8 \phi_1^3 + f_2 cos(\Omega T_0 + \tau_2) \end{aligned} \tag{13b}$$

The solution to (12) is given by

$$\eta_1 = P(T_2) e^{i \omega_1 T_0} + cc \tag{14a}$$

$$\phi_1 = Q(T_2) e^{i \omega_2 T_0} + cc \tag{14b}$$

where P and Q are complex quantities, and cc denotes complex conjugate of all preceding terms. Substitution of (14) into (13) gives secular terms in the RHS of (13). Particularly, in the presence of an internal resonance condition arising from quadratic nonlinearities ($\omega_2 \approx 2\omega_1$) and primary resonance ($\Omega \approx \omega_1$), the secular terms are collected and set to zero to obtain the solvability conditions

$$2 i \omega_1 (D_2 P + \mu_1 P) = \alpha_2 \bar{P} Q e^{i \sigma_1 T_0} + 3 \beta_1 P^2 \bar{P} + 2 \beta_3 P Q \bar{Q} + \frac{1}{2} f_1 e^{i(\sigma_2 T_2 + \tau_1)} \tag{15a}$$

$$2 i \omega_2 (D_2 Q + \mu_2 Q) = \alpha_4 P^2 e^{-i \sigma_1 T_0} + 3 \beta_8 Q^2 \bar{Q} + 2 \beta_6 P \bar{P} Q \tag{15b}$$

where the overbar denotes the complex conjugate, and σ_1 and σ_2 are detuning parameters, (measures of the closeness to the internal resonance condition and the primary resonance condition, respectively), given by

$$\omega_2 = 2 \omega_1 + \epsilon^2 \sigma_1 \tag{16a}$$

$$\Omega = \omega_1 + \epsilon^2 \sigma_2 \tag{16b}$$

Assuming P and Q to be of the form

$$P = \frac{1}{2} r_1(T_2) e^{i\psi_1(T_2)} \qquad Q = \frac{1}{2} r_2(T_2) e^{i\psi_2(T_2)} \tag{17}$$

where $r_i,\ \psi_i,\ (i = 1, 2)$ are real quantities that are functions of T_2, substituting (17) into (15), and separating the real and imaginary parts of the resulting equations give the differential equations for the evolution of $r_i,\ \psi_i,\ (i = 1, 2)$ as

$$4\omega_1(r_1' + \mu_1 r_1) - \alpha_2 r_1 r_2 \sin\nu_1 - 2f_1 \sin\nu_2 = 0 \tag{18a}$$

$$4\omega_2(r_2' + \mu_2 r_2) + \alpha_4 r_1^2 \sin\nu_1 = 0 \tag{18b}$$

$$8\omega_1 r_1 \psi_1' + 3\beta_1 r_1^3 + 2\beta_3 r_1 r_2^2 + 2\alpha_2 r_1 r_2 \cos\nu_1 + 4f_1 \cos\nu_2 = 0 \tag{18c}$$

$$8\omega_2 r_2 \psi_2' + 3\beta_8 r_2^3 + 2\beta_6 r_1^2 r_2 + 2\alpha_4 r_1^2 \cos\nu_1 = 0 \tag{18d}$$

where prime denotes differentiation with respect to T_2, and

$$\nu_1 = \sigma_1 T_2 + \psi_2 - 2\psi_1$$

$$\nu_2 = \sigma_2 T_2 + \tau_1 - \psi_1$$

The final solution (the time history of the modal coordinates) is given by

$$\eta(t) = \epsilon r_1(\epsilon^2 t) \cos(\Omega t + \tau_1 - \nu_2) \tag{19a}$$

$$\phi(t) = \epsilon r_2(\epsilon^2 t) \cos(2\Omega t + 2\tau_1 - 2\nu_2 + \nu_1) \tag{19b}$$

and may be written in terms of the original variables ζ and θ using (8).

The steady state amplitude of oscillations are obtained by setting $r_i' = \nu_i' = 0$ $(i = 1, 2)$ in (18) which reduce to

$$4\omega_1\mu_1 r_1 - \alpha_2 r_1 r_2 \sin\nu_1 - 2f_1 \sin\nu_2 = 0 \tag{20a}$$

$$4\omega_2\mu_2 r_2 + \alpha_4 r_1^2 \sin\nu_1 = 0 \tag{20b}$$

$$8\omega_1\sigma_2 + 3\beta_1 r_1^3 + 2\beta_3 r_1 r_2^2 + 2\alpha_2 r_1 r_2 \cos\nu_1 + 4f_1 \cos\nu_2 = 0 \tag{20c}$$

$$8\omega_2(2\sigma_2 - \sigma_1) + 3\beta_8 r_2^3 + 2\beta_6 r_1^2 r_2 + 2\alpha_4 r_1^2 \cos\nu_1 = 0 \tag{20d}$$

The coupled nonlinear equations (20) may be solved to obtain the frequency response plot which shows the steady state modal amplitudes r_1^{ss} and r_2^{ss} as a function of the detuning σ_2 (i.e. the forcing frequency Ω), as well as plots to understand the effect of the detuning σ_1 (which depends on the thermal protrusion 'α') on the steady state amplitude. The solutions to (20) are obtained numerically and presented in the results and discussion section.

2. Secondary Resonance

For the nonresonant case (Ω far away from ω_1 or ω_2) the ordering is to be chosen so that the forcing term appears at order ϵ, while the damping and nonlinearities appear at order ϵ^3. In addition, to include the case of combination resonances which occur when the forcing consists of a multifrequency excitation, a two frequency excitation occurring at Ω_1 and Ω_2 ($\Omega_1 < \Omega_2$) is considered. Accordingly, the ordering of quantities is given by

$$\hat{\mu}_i = \epsilon^2 \mu_i \qquad A_j = \epsilon \alpha_j \qquad B_k = \beta_k \qquad \hat{F}_i = \epsilon(f_{i1}\cos(\Omega_1 t + \tau_{i1}) + f_{i2}\cos(\Omega_2 t + \tau_{i2})) \\ i = 1,2\ ; \quad j = 1,2\ldots,6\ ; \quad k = 1,2,\ldots,8 \tag{21}$$

Substituting (9), (10), (21) into (5) and collecting terms of order ϵ and order ϵ^3 gives

$$D_0^2\eta_1 + \omega_1^2\eta_1 = f_{11}cos(\Omega_1 T_0 + \tau_{11}) + f_{12}cos(\Omega_2 T_0 + \tau_{12}) \tag{22a}$$

$$D_0^2\phi_1 + \omega_2^2\phi_1 = f_{21}cos(\Omega_1 T_0 + \tau_{21}) + f_{22}cos(\Omega_2 T_0 + \tau_{22}) \tag{22b}$$

$$D_0^2\eta_3 + \omega_1^2\eta_3 = -2D_0D_2\eta_1 - 2\mu_1 D_0\eta_1 + \alpha_1\eta_1^2 + \alpha_2\eta_1\phi_1 + \alpha_3\phi_1^2 \\ + \beta_1\eta_1^3 + \beta_2\eta_1^2\phi_1 + \beta_3\eta_1\phi_1^2 + \beta_4\phi_1^3 \tag{23a}$$

$$D_0^2\phi_3 + \omega_2^2\phi_3 = -2D_0D_2\phi_1 - 2\mu_2 D_0\phi_1 + \alpha_4\eta_1^2 + \alpha_5\eta_1\phi_1 + \alpha_6\phi_1^2 \\ + \beta_5\eta_1^3 + \beta_6\eta_1^2\phi_1 + \beta_7\eta_1\phi_1^2 + \beta_8\phi_1^3 \tag{23b}$$

The solution to (22) is given by

$$\eta_1 = P(T_2)e^{i\omega_1 T_0} + \Gamma_{11}e^{i\Omega_1 T_0} + \Gamma_{12}e^{i\Omega_2 T_0} + cc \tag{24a}$$

$$\phi_1 = Q(T_2)e^{i\omega_2 T_0} + \Gamma_{21}e^{i\Omega_1 T_0} + \Gamma_{22}e^{i\Omega_2 T_0} + cc \tag{24b}$$

where

$$\Gamma_{ij} = \frac{f_{ij}e^{\tau_{ij}}}{2(\omega_i^2 - \Omega_j^2)^2} \qquad i = 1,2; \quad j = 1,2$$

The response for the nonresonant case consists of the forced response at the excitation frequencies Ω_1 and Ω_2 as well as the free response close to the system natural frequencies. Typically, the free response term decays to zero owing to system damping, however, under particular conditions and a suitable set of system parameters, the free response term does not decay but has a steady state amplitude for long time. This condition leads to a secondary resonance, and is the topic of investigation.

Substituting (24) into (23) reveals that additional secular terms appear in the RHS when the excitation frequencies are related to the linear natural frequencies by the following conditions

$$\begin{aligned}
\Omega_1 &\approx \frac{\omega_1}{3} & \Omega_2 &\approx \frac{\omega_1}{3} \\
\Omega_1 &\approx \frac{\omega_1}{2} & \Omega_2 &\approx \frac{\omega_1}{2} \\
\Omega_1 &\approx \frac{3\omega_1}{2} & \Omega_2 &\approx \frac{3\omega_1}{2} \\
\Omega_1 &\approx 2\omega_1 & \Omega_2 &\approx 2\omega_1 \\
\Omega_1 &\approx 3\omega_1 & \Omega_2 &\approx 3\omega_1 \\
\Omega_1 &\approx 4\omega_1 & \Omega_2 &\approx 4\omega_1 \\
\Omega_1 &\approx 5\omega_1 & \Omega_2 &\approx 5\omega_1 \\
\Omega_2 \pm \Omega_1 &\approx \omega_1 & \Omega_2 \pm \Omega_1 &\approx 3\omega_1 \\
2\Omega_1 \pm \Omega_2 &\approx \omega_1 & 2\Omega_2 \pm \Omega_1 &\approx \omega_1 \\
\Omega_2 - 2\Omega_1 &\approx \omega_1
\end{aligned} \tag{25}$$

$$\begin{aligned}
\Omega_1 &\approx \frac{\omega_2}{4} & \Omega_2 &\approx \frac{\omega_2}{4} \\
\Omega_1 &\approx \frac{\omega_2}{3} & \Omega_2 &\approx \frac{\omega_2}{3} \\
\Omega_1 &\approx \frac{\omega_2}{2} & \Omega_2 &\approx \frac{\omega_2}{2} \\
\Omega_1 &\approx \frac{3\omega_2}{4} & \Omega_2 &\approx \frac{3\omega_2}{4} \\
\Omega_1 &\approx \frac{3\omega_2}{2} & \Omega_2 &\approx \frac{3\omega_2}{2} \\
\Omega_1 &\approx 2\omega_2 & \Omega_2 &\approx 2\omega_2 \\
\Omega_2 \pm \Omega_1 &\approx \frac{\omega_2}{2} & \Omega_2 \pm \Omega_1 &\approx \frac{3\omega_2}{2} \\
\Omega_2 \pm \Omega_1 &\approx \omega_2 & \Omega_2 \pm \Omega_1 &\approx 2\omega_2 \\
2\Omega_1 \pm \Omega_2 &\approx \omega_2 & 2\Omega_2 \pm \Omega_1 &\approx \omega_2 \\
\Omega_2 - 2\Omega_1 &\approx \omega_2
\end{aligned} \tag{26}$$

Equations (25) and (26) only list conditions for which additional secular terms appear in the solvability conditions. The existence of a nontrivial solution to the solvability conditions implies the existence of nonzero free response, i.e. occurrence of a secondary resonance,

and it depends strongly on the system parameters. The focus in this paper is to identify excitation frequencies and their combinations that potentially lead to a secondary resonance. The existence of nontrivial solutions to the solvability conditions for each case is therefore not discussed.

IV. RESULTS AND DISCUSSION

The discussion pertains to results presented for the system parameters in Table I unless mentioned otherwise. The force displacement relation for the trailing end spring using these parameters is plotted in Fig 6 for the linear as well as nonlinear cases.

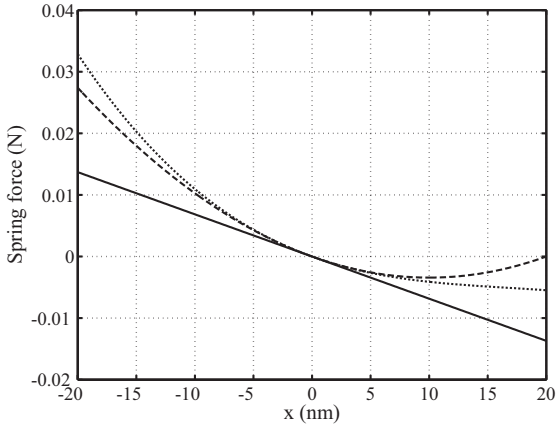

FIG. 6. Displacement-force plot for the trailing edge spring; $k_{21} = 3.3 \times 10^5$, $\alpha = 2.075$; — linear: $k_{11} = \alpha k_{21}$, $k_{12} = k_{13} = 0$; $--$ quadratic nonlinearity: $k_{11} = \alpha k_{21}$, $k_{12} \neq 0$, $k_{13} = 0$; $\cdots$ quadratic and cubic nonlinearity: $k_{11} = \alpha k_{21}$, $k_{12} \neq 0$, $k_{13} \neq 0$

A. Primary Resonance ($\Omega \approx \omega_1$)

1. *Linear Damped System ($k_{12} = 0$, $k_{13} = 0$)*

For the linear system (i.e. when nonlinearities are absent: $k_{12} = 0$, $k_{13} = 0$) the responses of the two modes η and ϕ are decoupled. The frequency response plot, which shows the steady state amplitude of oscillations as a function of detuning σ_2 (a measure of the closeness of to primary resonance condition) is shown by the dotted curves in Fig 7. For the linear damped case, the frequency response curve is always a single valued function of σ_2 and has

a peak in the first modal coordinate (η) at $\sigma_2 = 0$ corresponding to a resonance condition of the linear system. The steady state amplitude of forced oscillations in the second modal coordinate (ϕ) is small compared to that for η because the frequency of excitation Ω is far away from ω_2.

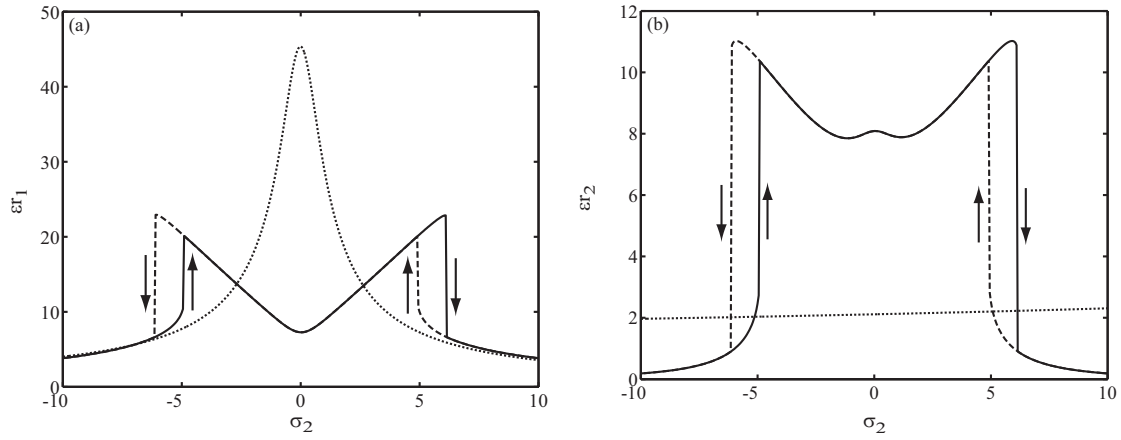

FIG. 7. Frequency response plot for the linear damped system and the damped system with only quadratic nonlinearities when $\omega_2 \approx 2\omega_1$ (a) First modal coordinate η (b) Second modal coordinate ϕ; $\cdots$ linear case; — nonlinear case with increasing σ_2; $--$ nonlinear case with decreasing σ_2

2. Nonlinear Damped System with only Quadratic Nonlinearities ($k_{12} \neq 0$, $k_{13} = 0$)

When nonlinearities of only the quadratic form are included ($k_{12} \neq 0$, $k_{13} = 0$), the frequency response curves for both modes can be significantly altered depending on the system parameters. Two important cases need consideration when nonlinearities are included: (a) when ω_2 is far away from $2\omega_1$ (no internal resonance), and (b) when $\omega_2 \approx 2\omega_1$ (internal resonance).

When ω_2 is far away from $2\omega_1$ (no internal resonance), the system modes are decoupled to first order, and the frequency response curves are equivalent to that of the linear case. However, when $\omega_2 \approx 2\omega_1$ (internal resonance), the frequency response curve is significantly altered from that of the linear case. The two modes become strongly coupled and the curve may become a multivalued function of σ_2 depending on system parameters. The frequency response plot is shown in Fig 7 when $\omega_2 \approx 2\omega_1$ (i.e. $\sigma_1 \approx 0$). It is evident that in certain ranges, for example, when $\sigma_2 \approx \pm 6$, there are two values at which the response could occur

for a given value of σ_2. The actual amplitude at which system response occurs is determined by the initial condition. A strong coupling of modes due to internal resonance leads to a much higher response in the second mode in the nonlinear case compared to the linear case. Additionally, the single peak in the first mode at $\sigma_2 = 0$ for the linear case is altered into two peaks at $\sigma_2 \approx \pm 6$ for the nonlinear case, implying that the largest response in the first mode occurs when Ω is slightly away from ω_1. As the system parameter σ_2 is changed (i.e the excitation frequency Ω is increased or decreased), the well known jump phenomena characteristic to nonlinear systems occurs. When σ_2 is increased from the left the amplitude of steady state oscillations follows the solid line, and when σ_2 is decreased from the right the amplitude of steady state oscillations follows along the dashed line. Two jumps are evident in both cases (increasing and decreasing σ_2) corresponding to the region where the response curve is a multivalued function of σ_2. A jump occurs when the system moves from a region of multivalued solutions to a region with unique solution as discussed below considering a damped system including cubic and quadratic nonlinearities.

3. Nonlinear Damped System with Cubic and Quadratic Nonlinearities ($k_{12} \neq 0$, $k_{13} \neq 0$)

For a damped system with cubic and quadratic nonlinearities ($k_{12} \neq 0$, $k_{13} \neq 0$), the frequency response curve depends on whether internal resonance occurs or not. An internal resonance could occur when $\omega_2 \approx 2\omega_1$ arising from quadratic nonlinearities, or when $\omega_2 \approx 3\omega_1$ arising from cubic nonlinearities. In this work the focus is on the first case as it is relevant to the values of ω_1 and ω_2 typically observed in the problem of slider-ABS systems with thermal protrusion.

When internal resonance is absent (ω_2 is far away from $2\omega_1$), the two modes are decoupled to first order. The response of the second mode (ϕ) is the same as that for linear forced response shown in Fig 7b. However, the response of the first mode (η) is altered from the linear response as shown in Fig 8. The effect of the cubic nonlinearity is to bend the linear response curve (to the right, because the cubic nonlinearity stiffens the system in this case), and the curve may become a multivalued function of σ_2. The curve presented for the nonlinear case in Fig 8 is obtained from an analytical closed form expression derived in [25]. As σ_2 is increased from the left, the steady state amplitude of oscillations change along the curve $ABCEF$, while the steady state amplitude of oscillations trace the curve

$FEDBA$ as σ_2 is decreased. The jump down CE in the forward direction, and the jump up DB in the reverse direction arise because the response curves move from a region of σ_2 where multiple solutions exist, to a region where only a unique solution exists to the response amplitude. The difference in the location of the jumps for increasing and decreasing σ_2 leads to a hysteresis loop. The portion DC of the response curve which lies in the hysteresis loop corresponds to unstable equilibria of (20) that are not physically realizable. The jumps in Fig 7 are similar to the jumps in Fig 8. In Fig 7, the branch of unstable equilibria between the two hysteresis loops (similar to the portion DC of Fig 8) is not shown because it is not detected by the simple numerical scheme used in this work to compute the equilibria of (20).

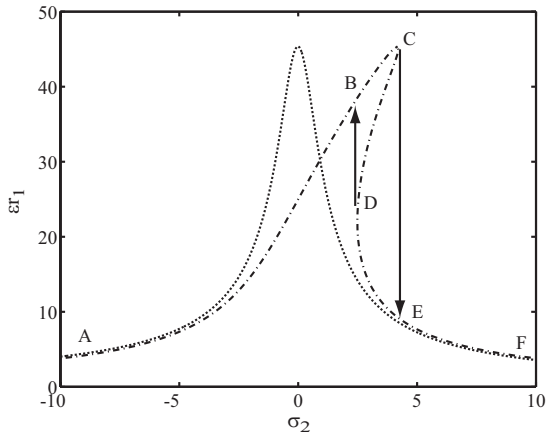

FIG. 8. Frequency response plot for the first modal coordinate η; $\cdots$ linear damped case; $-\cdot-$ damped case with cubic nonlinearities but no internal resonance

When an internal resonance occurs ($\omega_2 \approx 2\omega_1$), the two modes get strongly coupled. The frequency response curves for this case are shown in Fig 9. The amplitude of the second mode is significantly higher in this case even when the excitation frequency is far away from ω_2. Comparing the frequency response curves for the first mode with previous cases, it is noted that the response curve for this case is similar to that in Fig 7 with the two peaks altered in amplitude and bent (to the right) because of the inclusion of cubic nonlinearities. The jump occurring near $\sigma_2 = 0$ for the chosen set of parameters is of particular interest because it implies that when Ω is close to ω_1, as would happen in the slider-ABS system model where the lubricant rippling occurs close to the first pitch mode frequency for the slider, a very small change in Ω could lead to a very large change in the resulting amplitude

of oscillations. Depending on other system parameters, the detuning between the lubricant rippling frequency Ω and the first pitch mode frequency ω_1 dictates whether the slider has a large amplitude response or a suppressed amplitude response suggesting a good explanation for the suppressed amplitude of slider vibrations observed in experiments.

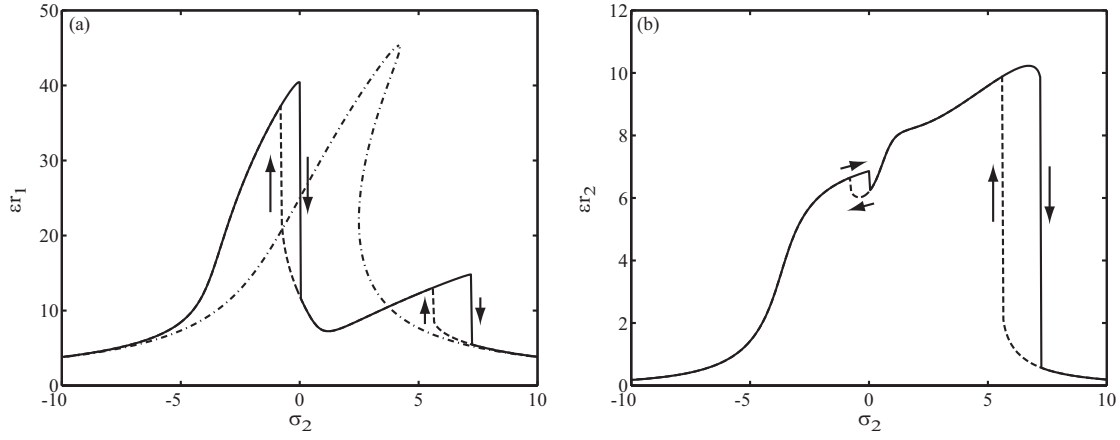

FIG. 9. Frequency response plot for the damped system with quadratic and cubic nonlinearities (a) First modal coordinate η (b) Second modal coordinate ϕ; $-\cdot-$ no internal resonance; — internal resonance ($\omega_2 \approx 2\omega_1$) with increasing σ_2; $--$ internal resonance ($\omega_2 \approx 2\omega_1$) with decreasing σ_2

The frequency response curves are plotted in Fig 10 for various values of α (the measure of thermal protrusion). Noting that changing α changes the detuning σ_1 (Fig 11), these plots may also be viewed as frequency response curves for changing σ_1 (a measure of closeness to the internal resonance condition $\omega_2 = 2\omega_1$). In Fig 10, by fixing the excitation frequency at say $\Omega = \omega_1$ ($\sigma_2 = 0$), it is seen that the amplitude of oscillations for particular values of α (or σ_1) are given by the points where the line $\sigma_2 = 0$ (the *ordinate*) intersects the frequency response curves. In particular, from Fig 10, it is evident that for $\alpha = 2.000$ and $\alpha = 2.075$ the *ordinate* intersects the frequency response curves at two points, but for $\alpha = 2.150$ the *ordinate* intersects the frequency response curves at only one point. The locus of the points of intersection of the frequency response curves with $\sigma_2 = 0$ is plotted as a function of σ_1 in Fig 12, where the solid and dashed lines denote the points of intersection of the *ordinate* with the solid and dashed lines, respectively, in frequency response curves of Fig 10. The plots reveal that near $\sigma_1 \approx 0$, a very slight change in σ_1 could lead to a very large change in the amplitude of oscillations. Particularly, increasing σ_1 above zero results in a sudden drop in the amplitude of oscillations of the first mode. This result is very interesting because it

implies that for the slider-ABS system, assuming that the excitation frequency (lubricant rippling Ω) is perfectly tuned to the ABS first pitch mode ω_1, a small change in the thermal protrusion could lead to a sudden suppression of slider vibration amplitude, offering a very plausible explanation of the suppressed vibration 'stable' zone seen in experiments at high heater power.

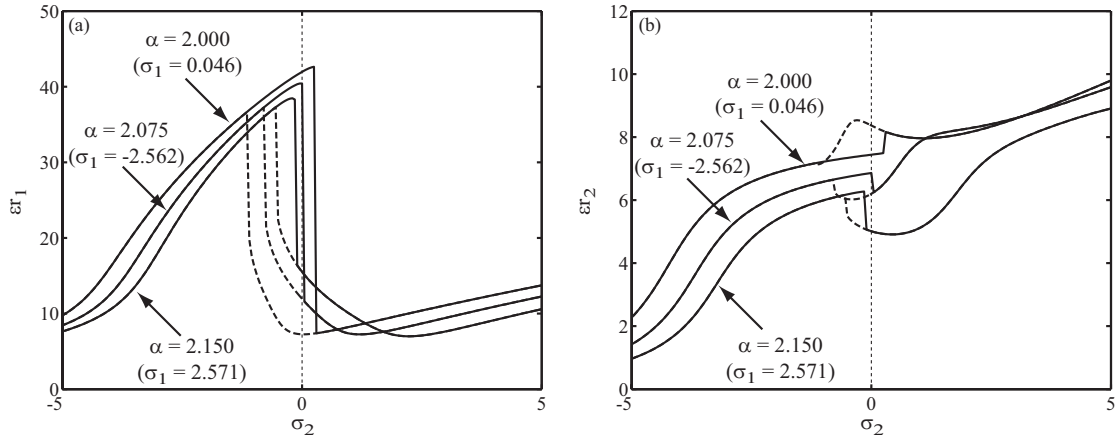

FIG. 10. Frequency response plot for the damped system with quadratic and cubic nonlinearities showing the effect of α; — internal resonance ($\omega_2 \approx 2\omega_1$) with increasing σ_2; $--$ internal resonance ($\omega_2 \approx 2\omega_1$) with decreasing σ_2

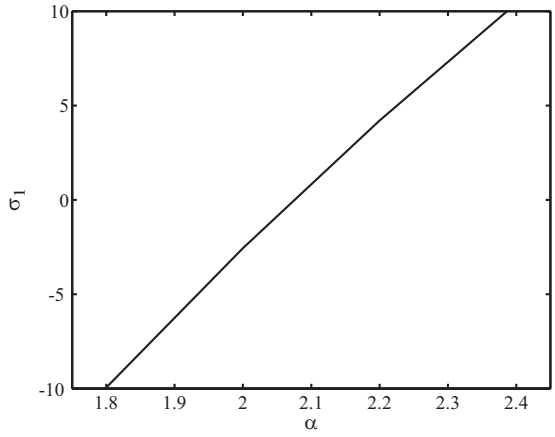

FIG. 11. Effect of thermal protrusion 'α' on the internal resonance detuning parameter 'σ_1'

Similar plots are shown in Fig 13 for $\sigma_2 = \pm 0.5$. It is interesting to note that when $\sigma_2 = -0.5$, an increase in σ_1 does not lead to a downward jump in the amplitude of oscillations of the first mode. Such a condition may also occur for a different set of system parameters even

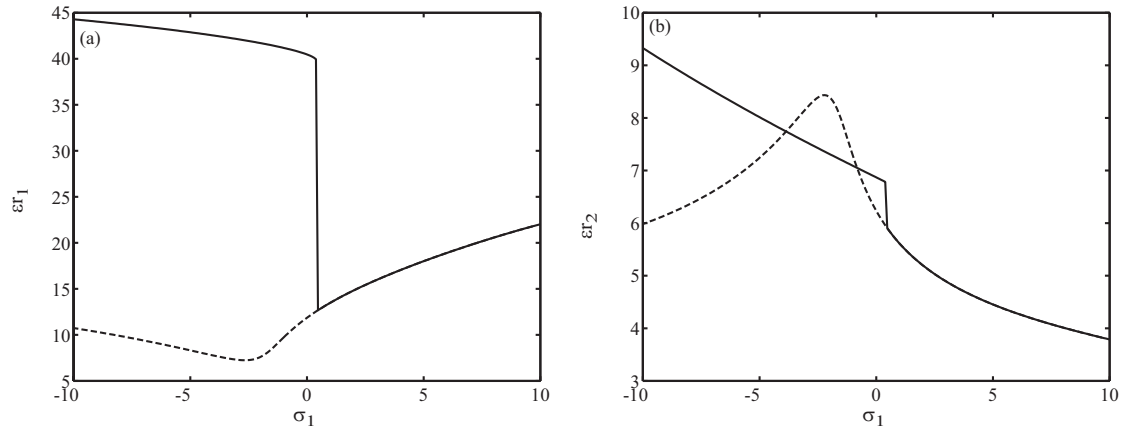

FIG. 12. Response amplitude as function of σ_1 for $\sigma_2 = 0$ for the damped system with quadratic and cubic nonlinearities (a) First modal coordinate (b) Second modal coordinate

when $\sigma_2 = 0$. In other words, certain slider designs may not exhibit the sudden suppression in vibrations for increasing thermal protrusion. The experimental results for one such case is shown in Fig 14, where an increase in heater power beyond the TDP does not show any suppression of the slider vibrations or AE signal.

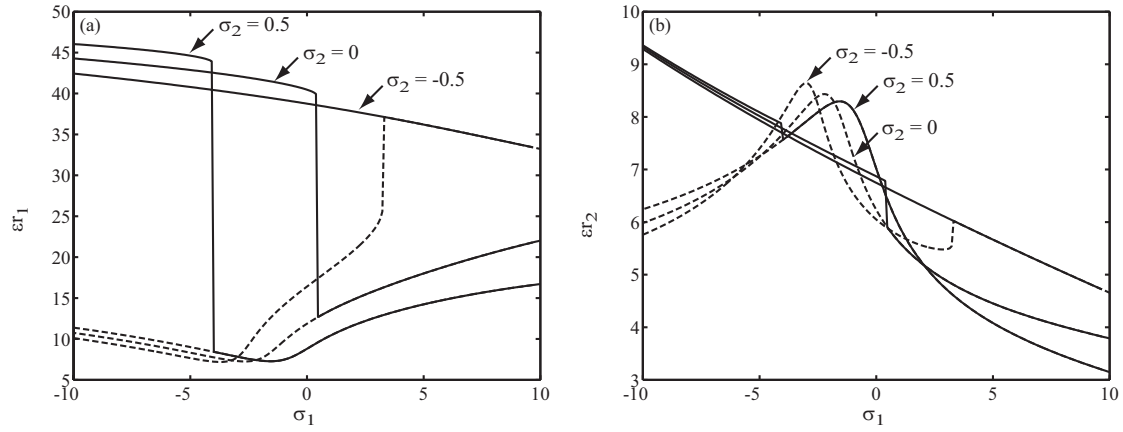

FIG. 13. Response amplitude as function of σ_1 for the damped system with quadratic and cubic nonlinearities showing the effect of σ_2 (a) First modal coordinate (b) Second modal coordinate

The time histories of responses are plotted in Fig 15 for the linear case, and the two solutions for the nonlinear case when $\alpha = 2.075$ ($\sigma_1 = .0463$) and $\sigma_2 = 0$. The amplitudes of oscillations (ζ,θ) are much smaller for one solution of the nonlinear case and corresponds to the case of suppressed vibrations.

The key findings from the foregoing nonlinear analysis may be summarized to explain

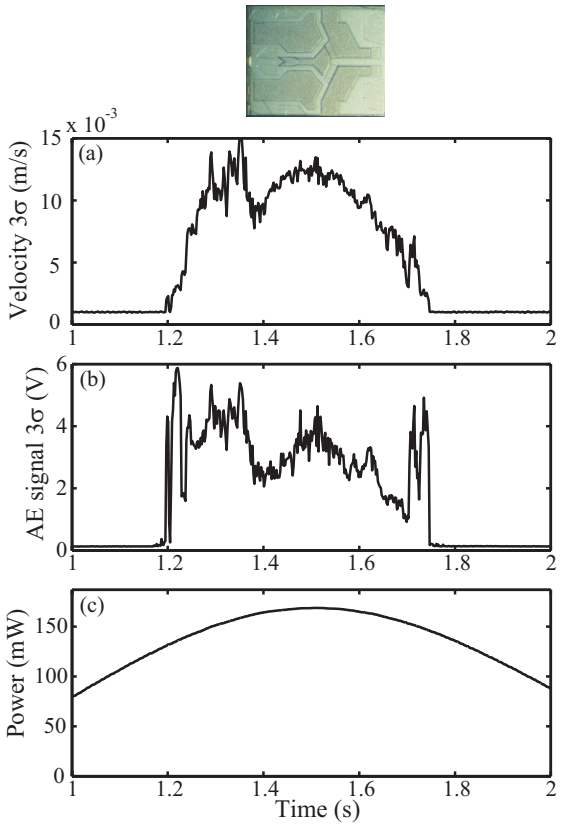

FIG. 14. Experimental result for the 'femto' slider: Time history of (a) slider's vertical velocity 3σ (b) AE signal 3σ (c) power supplied to TFC heater

the peculiar slider dynamics seen in experiments. When the thermal protrusion causes the natural frequencies of the slider-ABS system to pass through and internal resonance, the amplitude of vibrations can significantly increase because of an unfavorable coupling of modes. Depending on system parameters a further change in thermal protrusion can result in a sudden suppression of vibrations because of the way nonlinearities interact within the system.

The external force (F) and system damping can also have a dramatic influence on the amplitude of oscillations. To demonstrate this effect Fig 16 and Fig 17 show the frequency response plot for different values of external force and damping, respectively. The other system parameters used in this calculation are listed in Table I. It is evident from these figures that the occurrence as well as location of jumps, and the amplitude of oscillations is strongly influenced by the external force and damping. At a given damping percentage, a jump (multiple response amplitudes for a given σ_2) can occur only if the external force

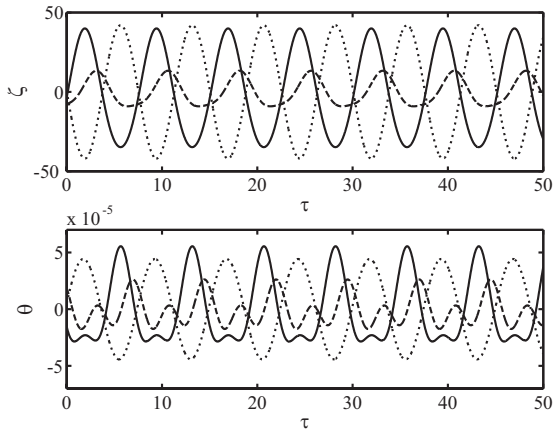

FIG. 15. Time history of response for linear damped system and damped system with quadratic and cubic nonlinearities when $\alpha = 2.075$ ($\sigma_1 = 0.046$) and $\sigma_2 = 0$; $\cdots$ linear case; — nonlinear case with large amplitude response; $--$ nonlinear case with suppressed amplitude response

amplitude is above a critical value, and similarly for a given external force amplitude, a jump can occur only if the damping is below a critical value. The magnitude of external force and damping, together with the frequency of the external forcing can therefore significantly alter the nonlinear system response.

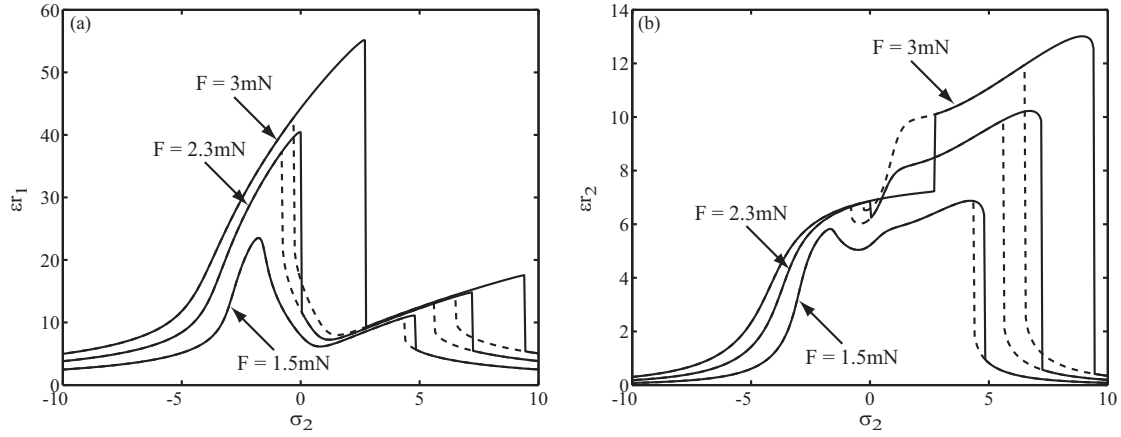

FIG. 16. Effect of external force on the frequency response plot for the damped system with quadratic and cubic nonlinearities and internal resonance ($\alpha = 2.075$) (a) First modal coordinate (b) Second modal coordinate

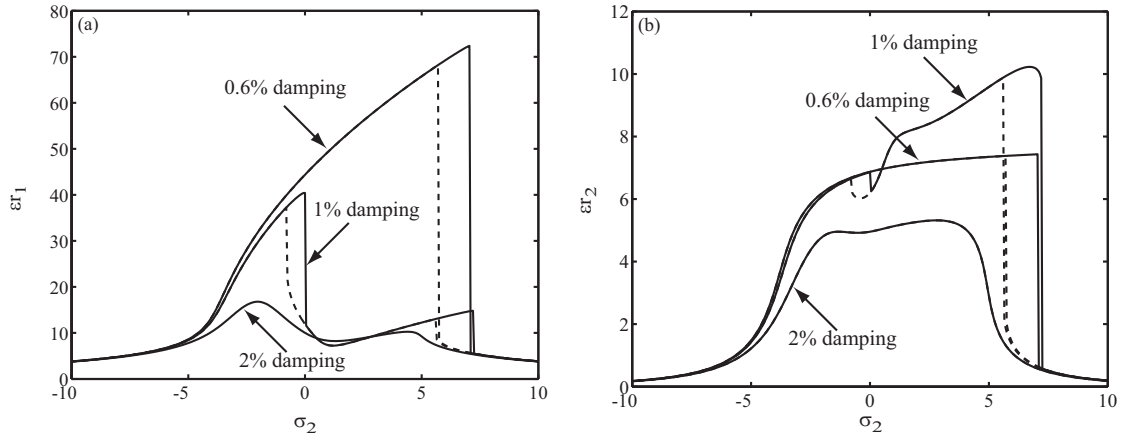

FIG. 17. Effect of damping on the frequency response plot for the damped system with quadratic and cubic nonlinearities and internal resonance ($\alpha = 2.075$) (a) First modal coordinate (b) Second modal coordinate

4. Dynamic Frequency Response Plots

The frequency response plots presented so far show the amplitude of oscillations at steady state as a function of σ_2. They are called the *stationary* frequency response curves, and are the solutions to the equilibrium equations (20) associated with the differential equations (18). The *dynamic* frequency response curves can be obtained by integration of (18) from σ_{2i} to σ_{2f} and assuming $\sigma_2 = \sigma_{2i} + sT_2$ where s is the rate of change of σ_2. These dynamic curves may be viewed as the envelop of the transient time history of oscillations of the two modes as σ_2 is increased or decreased (i.e. when passing through a resonance). The equilibrium solution of (20) with $\sigma_2 = \sigma_{2i}$ is used as the initial condition for this integration. The dynamic frequency response plots obtained in this manner are plotted for the case of only quadratic nonlinearities (Fig 18), and for the case of cubic as well as quadratic nonlinearities (Fig 19) for $s = 0.5$. It is evident that the dynamic curves follow the stationary curves fairly well but show oscillations after encountering a jump. Smaller values of s cause the dynamic curves to asymptote to the stationary curves, while larger values of s cause them to deviate from the stationary curves.

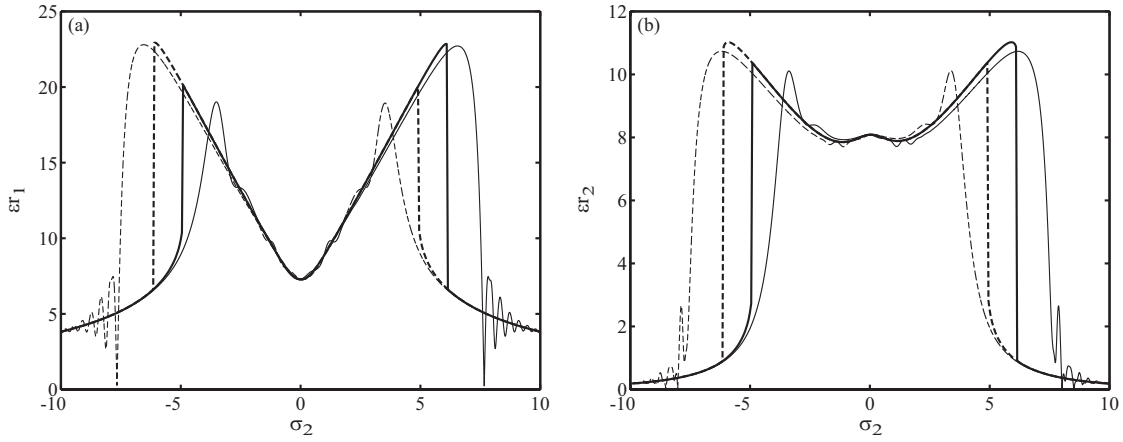

FIG. 18. Dynamic and stationary frequency response plot for the damped system with only quadratic nonlinearities and internal resonance ($\alpha = 2.075$) (a) First modal coordinate (b) Second modal coordinate; — increasing σ_2; $--$ decreasing σ_2; bold lines represent the *stationary* curves

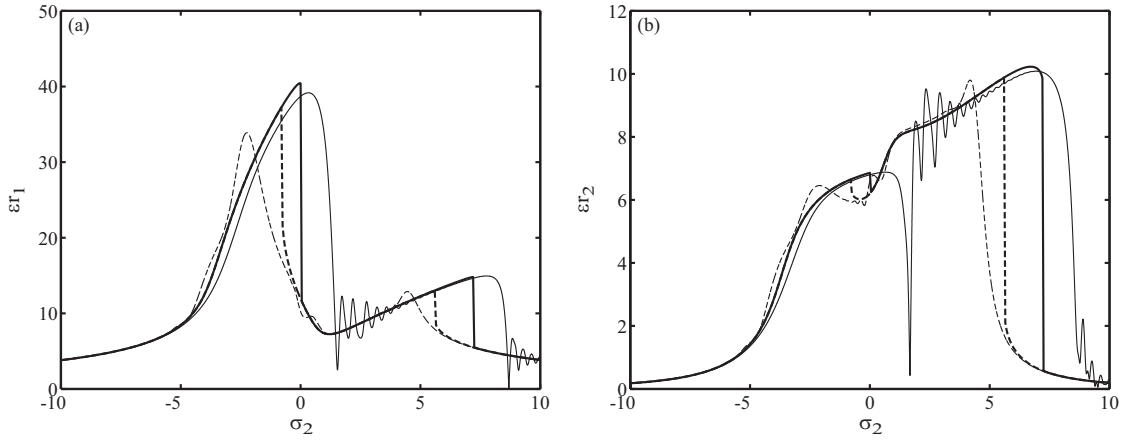

FIG. 19. Dynamic and stationary frequency response plot for the damped system with quadratic and cubic nonlinearities and internal resonance ($\alpha = 2.075$) (a) First modal coordinate (b) Second modal coordinate; — increasing σ_2; $--$ decreasing σ_2; bold lines represent the *stationary* curves

B. Secondary Resonance

For the nonresonant case (Ω far away from ω_1 or ω_2), the nonlinear analysis shows that when the excitation frequencies are related to ω_1 and ω_2 through one of the particular combinations listed in (25) and (26) a secondary resonance can potentially occur and result in interesting system dynamics.

For the two frequency excitation case considered in this work, two of the conditions in

(25) and (26) (also referred to as the secondary resonance conditions), can be satisfied simultaneously. Considering the special case of internal resonance ($\omega_2 \approx 2\omega_1$), the combinations under which two secondary resonance conditions are satisfied simultaneously are calculated. The final result is that two secondary resonance conditions are satisfied simultaneously when the excitation frequencies Ω_1 and Ω_2 are related to ω_1 through a multiplicative constant c and satisfy two of the conditions listed in (25) or (26). The actual manifestation of this secondary resonance is determined by the system parameters, and it occurs only when the solvability conditions for a simultaneous occurrence of secondary resonance has nontrivial solutions. The set of all possible values that the parameter c may take is listed below

$$c = 1, 2, 3, \ldots, 14 \tag{27a}$$

$$c = \frac{1}{3}(1, 2, 4, 5, 7, 8, 10, 11, 13, 14) \tag{27b}$$

$$c = \frac{1}{2}(1, 3, 5, 7, 9) \tag{27c}$$

$$c = \frac{1}{6}(5, 7) \tag{27d}$$

$$c = \frac{1}{4}(3, 5) \tag{27e}$$

$$c = \frac{1}{5}(1, 2, 3, 4, 6) \tag{27f}$$

For a three frequency excitation, three secondary resonance conditions can be satisfied simultaneously, and the list for c would include more values. When a secondary resonance does occur, the frequency spectrum of the system response consists of a free response close to the linear natural frequencies ω_m tuned by the nonlinearities in addition to the forced response at the excitation frequencies Ω_n. Since the forcing frequencies Ω_n are related to ω_m through various fractions c, the system response spectrum shows peaks corresponding to these *fractional harmonics*, which include *superharmonics* and *subharmonics* of the second and third order arising from the system quadratic and cubic nonlinearities, respectively [25].

The theoretical predictions of fractional harmonics arising from the two simultaneous secondary resonance conditions are shown in Table II. The value $\omega_1 = 128kHz$ is the experimentally observed ABS first pitch mode frequency for this slider-ABS system. All of the frequencies experimentally observed in the spectrum of slider vibrations (Fig 3) are well predicted by this theory. The only significant peak that appears in experimental results, but is not predicted from theory is at $233kHz$. Investigation reveals that this frequency corresponds to the fractional harmonic with $c = \frac{11}{6}$ and is predicted from theory if a three

term excitation is considered. It is pointed out that not all of the theoretically predicted frequencies are seen in the experiments. This is not surprising because even though a secondary resonance is potentially predicted from theory, it may not actually occur because nontrivial solutions to the solvability conditions do not exist for the chosen set of system parameters.

C. HDI Design Considerations

The results of the analytical work reveal important insight into the dynamics of a slider under the effect of thermal protrusion. It is shown that depending on the system parameters, the nonlinearities at the head disc interface in combination with thermal protrusion can lead to interesting system dynamics for particular ranges of protrusion. These include the strong coupling of modes through internal resonance leading to large amplitude oscillations, and the sudden suppression/increase in oscillation amplitude due to jump conditions.

An internal resonance can lead to a large amplitude slider response because of an unfavorable coupling of vibration modes, and this can result in slider-lubricant/disc contact or enhance existing slider-lubricant/disc contact. In order to avoid this condition, the ABS should be designed to have pitch mode frequencies such that $\omega_2 > 2\omega_1$ with zero heater power, so that thermal protrusion results in the system moving away from an internal resonance condition (because ω_2 increases and ω_1 remains largely unaffected by thermal protrusion). If $\omega_2 < 2\omega_1$ with zero heater power, it may be desirable to transition through the internal resonance condition in the low heater power range because in that case, the thermal protrusion is small and head-disc clearance is relatively large, leaving a greater margin to accommodate any large amplitude vibrations arising from an internal resonance. Internal resonance and the resulting large amplitude vibrations can also be used favorably, for example, by intentionally inducing internal resonance and detecting slider vibrations with a magnetic signal, one can ascertain the flying height of a slider.

Only the pitch and vertical degrees of freedom are considered in this work, but the analysis can be extended to a three degree of freedom model that includes slider roll. The internal resonance conditions for the three degree of freedom model are $\omega_m \approx 2\omega_n$ or $\omega_m \approx 3\omega_n$ for $m, n = 1, 2, 3$, and a coupling of modes as well as interesting system dynamics can occur when thermal protrusion leads to an internal resonance condition.

Experimental: $\omega_1 = 128kHz$		
$c = p/q$	$\Omega = c\ \omega_1$	Seen in Experiments?
1/5	26	
1/3	43	
2/5	51	
1/2	64	
3/5	77	
2/3	85	Yes
3/4	96	
4/5	102	
5/6	107	Yes
1	128	Yes
7/6	149	
6/5	154	
5/4	160	
4/3	171	
3/2	192	Yes
5/3	213	Yes
2	256	Yes
7/3	299	Yes
5/2	320	
8/3	341	Yes
3	384	Yes
10/3	427	
7/2	448	
11/3	469	
4	512	

TABLE II. Possible fractional harmonics when two secondary resonance conditions are simultaneously satisfied

This analytical study also highlights the role of lubricant rippling, or other periodic excitation in determining slider dynamics. Since a small difference in the frequency of the excitation and the first pitch mode frequency of the slider can result in very different amplitudes of response, it is inferred that the ability of the lubricant to ripple as well as recover/relax needs important consideration from the perspective of having favorable slider dynamics.

V. CONCLUSION

Slider instability and dynamics at touchdown/contact are investigated in this paper through experiments and analytical modeling. Experiments reveal that for certain slider designs, when the heater power is increased beyond a critical power above the TDP, the slider vibrations are suddenly suppressed. A simple two degree of freedom model that accounts for nonlinearities at the HDI through quadratic and cubic approximations is used to analytically investigate the interesting features of this problem. It is shown that the thermal protrusion induced by the heater power can cause the system modes to couple unfavorably for certain heater power ranges. This condition can manifest as large amplitude slider vibrations and result in slider-lubricant/disc contact or enhance the existing slider-lubricant/disc contact. System nonlinearities can also lead to a favorable suppression/reduction of slider vibration amplitudes through the jump phenomena characteristic to many nonlinear systems. Excitation frequencies that result in large amplitude slider vibrations, and the dominant frequencies at which slider response occurs are also predicted from theory, and they are in excellent agreement with experimental results. The theoretical analysis in this work highlights HDI design considerations that can prevent slider instability as well as mitigate unwanted slider vibrations ensuring HDI reliability at extremely low head-disc clearance.

---

[1] R.-H. Wang, V. Nayak, F.-Y. Huang, W. Tang, and F. Lee, Journal of Tribology, **123**, 561 (2001).

[2] B. Knigge and F. E. Talke, Tribology International, **34**, 453 (2001).

[3] J. Kiely and Y.-T. Hsia, Journal of Tribology, **128**, 525 (2006).

[4] J. Kiely and Y.-T. Hsia, Microsystem Technologies, **14**, 403 (2008).

[5] J. Xu, J. Kiely, and Y.-T. Hsia, Microsystem Technologies, **15**, 687 (2009).

[6] B. H. Thornton and D. B. Bogy, IEEE Transactions on Magnetics, **39**, 722 (2003).

[7] B. H. Thornton and D. B. Bogy, IEEE Transactions on Magnetics, **39**, 2420 (2003).

[8] M. C. Mate, P. C. Arnett, P. Baumgart, Q. Dai, U. M. Guruz, B. E. Knigge, R. N. Payne, O. J. Ruiz, G. J. Wang, and B. K. Yen, IEEE Transactions on Magnetics, **40**, 3156 (2004).

[9] J. Xu, H. Kohira, H. Tanaka, and S. Saegusa, IEEE Transactions on Magnetics, **41**, 3031 (2005).

[10] R. Ambekar, V. Gupta, and D. B. Bogy, Journal of Tribology, **127**, 530 (2005).

[11] V. Gupta, PhD Thesis, University of California Berkeley (2007).

[12] D. Chen, PhD Thesis, University of California Berkeley (2008).

[13] Q. Dai, B. E. Knigge, R. J. Waltman, and B. Marchon, IEEE Transactions on Magnetics, **39**, 2459 (2003).

[14] Q. Dai, F. Hendriks, and B. Marchon, Journal of Applied Physics, **96**, 696 (2004).

[15] B. Marchon, T. Karis, Q. Dai, and R. Pit, IEEE Transactions on Magnetics, **39**, 2447 (2003).

[16] R. Ambekar and D. B. Bogy, Applied Physics Letters, **92**, 2008 (2008).

[17] S. Moseley and D. B. Bogy, IEEE Transactions on Magnetics, **45** (2009).

[18] M. C. Mate, B. Marchon, A. N. Murthy, and S.-H. Kim, Tribology Letters, **37**, 581 (2010).

[19] S. Vangipuram Canchi and D. Bogy, IEEE Transactions on Magnetics, **46**, 764 (2010).

[20] B. Liu, M. S. Zhang, S. K. Yu, W. Hua, C. H. Wong, W. D. Zhou, Y. J. Man, L. Gonzaga, and Y. S. Ma, Journal of Magnetism and Magnetic Materials, **320**, 3183 (2008).

[21] J. Zheng and D. Bogy, Tribology Letters (accepted) (2010).

[22] S. K. Yu, B. Liu, W. D. Zhou, W. Hua, and L. Gonzaga, IEEE Transactions on Magnetics, **45**, 4979 (2009).

[23] B. Liu, M. S. Zhang, S. K. Yu, W. Hua, Y. S. Ma, W. D. Zhou, L. Gonzaga, and Y. J. Man, IEEE Transactions on Magnetics, **45**, 899 (2009).

[24] A. I. Vakis, S.-C. Lee, and A. Polycarpou, IEEE Transactions on Magnetics, **45**, 4966 (2009).

[25] A. H. Nayfeh and D. T. Mook, *Nonlinear oscillations* (John Wiley & Sons, New York, 1979).